https://doi.org/10.1016/j.tust.2018.11.013

Imaging and Condition Diagnosis of Underground Sewer Liners via Active and Passive Infrared Thermography: a case study in Singapore

Janet F.C. SHAM*[,a], Wallace W.L. LAI[a], Wing CHAN[b], Chee Lin KOH[b]
[a] Department of Land Surveying and Geo-informatics, The Hong Kong Polytechnic University, Hong Kong
[b] Singapore's Pipeline Inspection and Services Company
Phone: +852 3400-8960; Fax: +852 2330 2994; email: wllai@polyu.edu.hk

Abstract

This paper presents a case study of customizing an in-house built In-pipe Infrared Thermographic System (IPITS), which makes use of thermo-images for imaging and diagnosis of pipe crown condition in underground sewer pipelines. Active and passive infrared thermography (IRT) were attempted in two gravity sewer pipes in Singapore in July 2017. The results show that images captured with active IRT (with heating) can image and unfold invisible lining defects not readily revealed by traditional visual inspection using CCTV. These defects include bubbles, wrinkling and delamination, or construction details (like anchor knobs in HDPE material), for which sizes were estimated using an image processing algorithm customized in an in-house program. Whilst images captured by passive IRT (without heating) can be used to identify suspected water seeping points, this paper also reports the design of instrumentation and appropriate parameter settings. The results of this case study are believed to pave the way for parallel inspections using a combination of CCTV and infrared cameras.

Keywords: infrared thermography, defect identification, condition assessment, sewer liners

Introduction

Nowadays, as in many metropolitan cities across the world, the underground environment of Asia's densely populated cities consists of extensive arrays of utilities networks. All these utilities networks serve our daily life through the provision of sewers, mains water, natural gas, telecommunications and electricity, among other things. However, all these utilities have their limit of service life; and hence it is crucial to assess their condition throughout their life cycle before any accidents occur due to deterioration. However, accidents may sometimes occur. For example, when the leakage from a sewage pipe or water pipe triggers soil erosion and causes a road to collapse without any warning [1], or the leakage of gas pipe may cause an explosion [2]. Such problems disturb our daily life through occurrences such as the cutting off of services provided by the utilities network. Therefore, it is necessary to carry out studies aimed at developing different technologies for condition assessment of underground utilities. Condition assessment results help utilities companies and their engineers to plan maintenance schedules and rehabilitation works for underground utilities before failures occur.

In the past decades, many technologies have been developed and used for condition assessment of underground utilities such as the following: (1) closed-circuit television (CCTV) and an advanced visual method specifically for pipeline condition assessment, (2) sewer scanning and evaluation technology, (3) acoustic methods such as ultrasonic (sonar) techniques, and lately some advanced methods such as (4) laser-based scanning and (5) ground penetrating radar. Beyond the above techniques, IRT is one of the possible methods for pipeline condition assessment that has attracted less attention [3]. Infrared thermography has been commonly used in the building industry during the past decade for debond detection on external façades of buildings. The principle of using IRT for debond detection is based on differences in the heat transfer mechanism evidenced in areas

with debond when compared with intact areas. It can also be used for detecting incidences of debond between liners and pipes. However, one of the major limitations of IRT is its inability to work under water, so it can only be used to study liner delaminations in the pipe crown where the surface is exposed to the air. Two gravity sewer pipes in Singapore were chosen for this trial. This paper presents a study of the application of rapid infrared thermography (IRT) techniques for pipeline condition assessment. The design of equipment and appropriate parameter settings are presented together with the results of on-site experiments.

1. Common Techniques for Condition Assessment of Pipeline

There are several methods for condition assessment of pipelines available in the market. The following section will focus on those used by the largest group of agencies in the pipeline industry. The riskiest method is always that requiring human entry into the underground environment and the application of the following methods reduces that need.

1.1. Closed-Circuit Television (CCTV)

Closed-circuit television (CCTV) is the most common technique for pipeline condition assessment. The apparent advantage of CCTV is that it is a technically simple method which can directly capture illuminated images of defects on the pipe's interior wall. When necessary, the captured images can be examined in detail by further zooming the camera from different angles by controlling the tractor. CCTV was first introduced in 1960s for the inspection of pipe interiors and it consists of a small optical camera mounted on a tractor, which is a self-propelled platform with wheels. Nowadays, high-definition cameras permit the capture of better images for interpretation and the system is remotely controlled by an operator on the ground surface. The natural limitation of CCTV is that it can only be applied above the water's surface and the

movement of the CCTV tractor along the pipe may affect the quality of captured images [4]. Besides, it can only determine defects that are already exposed on the surface of the pipe's interior wall. The interpretation of collected images is highly subjective, which largely depends on the experience of the interpreter, any factors such as uneven and inadequate lighting may also affect the interpretation. About 2% of the main sewer network in the UK had been surveyed by 2004 and at least 20% of those observations obtained by CCTV survey were thought to be inaccurate [5].

1.2. Ultrasonic (Sonar) Technique

Ultrasonic techniques can be used to measure mass loss of exposed steel bars due to corrosion, and can also identify deformation of pipes and the volume of debris inside a pipeline. The basic principle of sonar techniques is that a sound wave is excited from a transmitter, and the time for transmission and reflection is measured. The distance of the transmitter from the target can then be estimated by using the speed of sound travelling in the medium, e.g. water, where a sonar profiling image of a pipe's interior condition can be constructed and assessed [3]. The advantage of sonar technique is that they are not limited to pipelines that are free of fluids, which largely removes the cost of dewatering and reduces the possibility of uninspected pipelines [6]. It is important to note that sonar images captured above and below the water surface should be constructed and interpreted separately because the travelling speed of sound in air and water are different [7].

1.3. Sewer Scanning and Evaluation Technology (SSET)

Optical scanner and gyroscope techniques were adapted for pipe interior inspection in the late 1990s, and integrated as Sewer Scanning and Evaluation Technology (SSET), specially developed for pipe interior condition survey. Unlike CCTV, SSET allows defect interpretation after the device has finished running through the whole length of pipe. This technology increases the

inspection efficiency, but requires an experienced analyst for interpretation. There is no possibility of local re-evaluation of suspicious defects once the survey is finished. There are studies in the literature on automating the assessment process in order to increase the efficiency and interpretation accuracy [8]. Similar to CCTV, SSET also involves interpretation of visual images collected by the device and only surface defects can be assessed. Therefore, SSET has recently been combined with other inspection techniques such as Ground Penetrating Radar (GPR) [9].

1.4. Laser-Based Scanning

Laser-based scanning has started to be employed for pipeline inspection in the early 21st century. The basic principle of laser-based scanning is that it will continuously generate a laser beam, which is projected around the pipe interior. It highlights and profiles the crown shape at every point along the pipe alignment [10, 11]. The limitation of laser-based scanning survey is that it can only be used reliably above. Recently, 3D laser scanning and modelling has been developed, which makes it possible to provide a 3D profile of the pipe [12].

2. Infrared Thermography

2.1. Infrared Thermography (IRT) for debond detection

Infrared thermography is a relatively mature non-destructive technique that has already been used in different engineering fields such as mechanical engineering, civil engineering, aerospace engineering and even medical engineering [13-16]. Lots of studies have already been conducted on the application of IRT to assess composite construction materials and structural integrity [17-25]. IRT measures any surface temperature difference/change by using an infrared sensor. An infrared camera can also be called a “radiometer”, which receives infrared radiation and provides thermal images with temperate data in each pixel. It is important to note that IRT measures relative

but not absolute temperature. Absolute temperature can only be obtained when parameters such as distance between the camera and lens, object emissivity and environmental factors such as the surrounding reflective temperature, wind speed and atmospheric humidity, are known[26]. IRT can be divided into passive and active thermography, where passive thermography involves the detection of surface temperature differences on the target object without any external heat source, such as in water seepage inspections. Active thermography uses a controllable external heat source that is applied to induce a surface temperature difference for purposes of detection [27]. Active thermography is a more flexible technique than passive thermography because of the availability of different combinations of excitation methods, modes of excitation and duration of excitation [26-30]. For debond detection, active heat sources are usually manipulated and controlled in order to elevate the temperature of the composite and then observe the subsequent spatial and temporal changes of temperature. The change of surface temperature of a thick, semi-infinite and opaque object after thermal excitation can be described by a three-dimensional heat conduction equation in the following differential form for nondestructive testing [26]:

$$C\rho \frac{\partial T}{\partial t} = \frac{\partial}{\partial x}\left(k_x \frac{\partial T}{\partial x}\right) + \frac{\partial}{\partial y}\left(k_y \frac{\partial T}{\partial y}\right) + \frac{\partial}{\partial z}\left(k_z \frac{\partial T}{\partial z}\right) \qquad \textbf{Equation 1}$$

where C is specific heat (J kg^{-1} K^{-1}), q is density (kg m^{-3}), 'T' is temperature (K), 't' is lapsed time and k_x, k_y, k_z (Wm^{-1} K^{-1}) are the anisotropic thermal conductivities in the three principal directions of heat transfer in the material. If thermal conductivities are the same in all three principal directions (i.e. kx = ky = kz), thermal diffusivity a (in m^2s^{-1}) = $k(C\rho)^{-1}$, then Equation 1 can be further simplified to Equation 2:

$$\frac{\partial^2 T}{\partial x^2} + \frac{\partial^2 T}{\partial y^2} + \frac{\partial^2 T}{\partial z^2} = \frac{1}{\alpha}\frac{\partial T}{\partial t} \qquad \textbf{Equation 2}$$

Both Equation 1 and Equation 2 models the heat transfer in a solid body by heat conduction.

Any discontinuity inside an object affects the cooling rate on the surface. Assuming a heat pulse is exerted on the surface of an object, the surface temperature change is described as follows, (i.e. z=0) [31]:

$$T(z = 0, t) = \frac{W}{e\sqrt{\pi t}} \qquad \textbf{Equation 3}$$

where W is the absorbed heat energy (Jm^{-2}), z (m) is the depth into the material, and *e* is the thermal effusivity ($\mathbf{W \bullet \sqrt{(s)} \bullet m^{-2} \bullet K^{-1}}$) of the material, which indicates the ability of a material to increase its temperature as a response to a given energy input. This change of temperature varies with different materials. It changes very fast in materials with higher effusivity (e.g. aluminum alloy) while it is slow in low effusivity materials (e.g. glass fibre plastic). The thermal effusivities of common materials are listed in Table 1:

Table 1: Thermal effusivity of common materials (extracted from source:[26])

Material	Effusivity ($\mathbf{W \bullet \sqrt{(s)} \bullet m^{-2} \bullet K^{-1}}$)
Air	9.19
Rubber	536
Glass fiber plastic	832
Water	1570
Concrete	1740
Aluminum alloy	20700

For capturing rapid temperature change in high effusivity materials, high speed (i.e. capturing frequency ≥ 30Hz) infrared cameras are usually applied. On the other hand, high thermal sensitivity infrared cameras (i.e. ≤0.05^{o}C) are usually used to capture the small temperature

changes occurring in relatively thermal reluctant materials e.g. concrete/composite materials [26]. Therefore, the thermal properties of testing materials were considered while designing the In-pipe Infrared Thermography System (IPITS) as shown in the following section.

3. Design of In-pipe Infrared Thermography System (IPITS) for Lining Debond Detection

3.1. Design of In-pipe Infrared Thermography System (IPITS) for Lining Debond Detection

The In-Pipe Infrared Thermography System (IPITS) consists of a self-propelled tractor, an infrared camera (FLIR Tau 2 640), a heat blower (for active thermography) and post-processing software as shown in the following Figure 1:

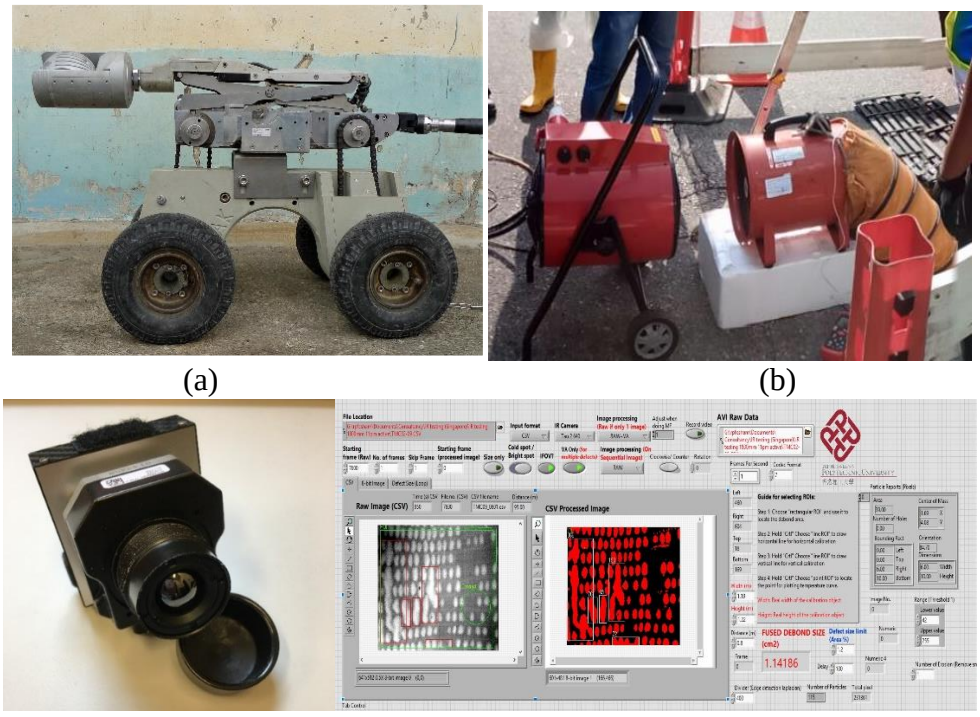

Figure 1: Photos of components of IPITS: (a) self-propelled tractor; (b) heat blower; (c) Infrared camera Flir Tau 2 640; (d) Post-processing platform.

A self-propelled tractor with visual recording facilities is usually used for CCTV surveys of gravity sewer pipes. In this study, CCTV survey was designed to work together with Infrared Thermography Survey. The infrared camera FLIR Tau 2 640 is an uncooled Microbolometer with a digital display of 640x512 pixels in NTSC format. The spectral band of this camera is 7.5-13.5μm and the ideal detecting temperature range for high gain is -25^{o}C to +135^{o}C. The thermal sensitivity is <50mK and the spatial resolution (instantaneous field of view, IFOV) is 1.889mrad with a 9mm lens. The frequency for data capture is 7.5Hz for the NTSC format. The IPITS also includes an in-house developed post-processing software package specifically designed for debond detection. It enables continuous measurement of size estimation in the captured thermal images.

4. On-site Experimental Setup

Two site trials were carried out in sewer pipes located at Jalan Eunos and Tech Park Crescent, Singapore, which were selected by the Singaporean Public Utility Board (PUB). The 900mm sewer pipe was rehabilitated using a high-density polyethylene (HDPE) liner fixed using adhesive, while the 1800mm sewer pipe is of the built-in (anchor knob sheet) AKS HDPE type. AKS is a form of anchor knob sheet as shown in Figure 2:

Figure 2: Anchor knob sheet (AKS) HDPE pipe liner installed inside the 1800mm sewer pipe.

The details of the trial tests are presented in the following Table 2:

Table 2: Details of site condition

	Jalan Eunos	Tech Park Crescent

Pipe diameter	1800mm		900mm	
Survey length	63.3m		104.6m	
Lining material	AKS HDPE		HDPE	
Thermography type	Active Thermography	Passive Thermography	Active Thermography	Passive Thermography
Date	26th July, 2017	26th July, 2017	26th July,2017	25th July, 2017
Time	2:20	00:10	15:20	15:20
Speed of tractor	6m/min	6m/min	6m/min	12m/min
Sewer Temperature	30.2	30.2	31.5	31.5
Liner Temperature	29.9	29.9	31.3	31.3
Heat time	30 mins	-	30 mins	-
Sewer Temperature (After heating)	34.5	-	33.1	-
Sewer Temperature (After heating)	34.7	-	33.3	-
Wind speed inside the pipe	-		0.5m/s	

Both passive and active thermography were carried out in both sewer pipes. There was no external heat stimulator used during the passive thermography survey, whereas a heat blower was used during the active thermography survey. The position of the infrared camera and the tractor is shown in the following schematic diagram Figure 3:

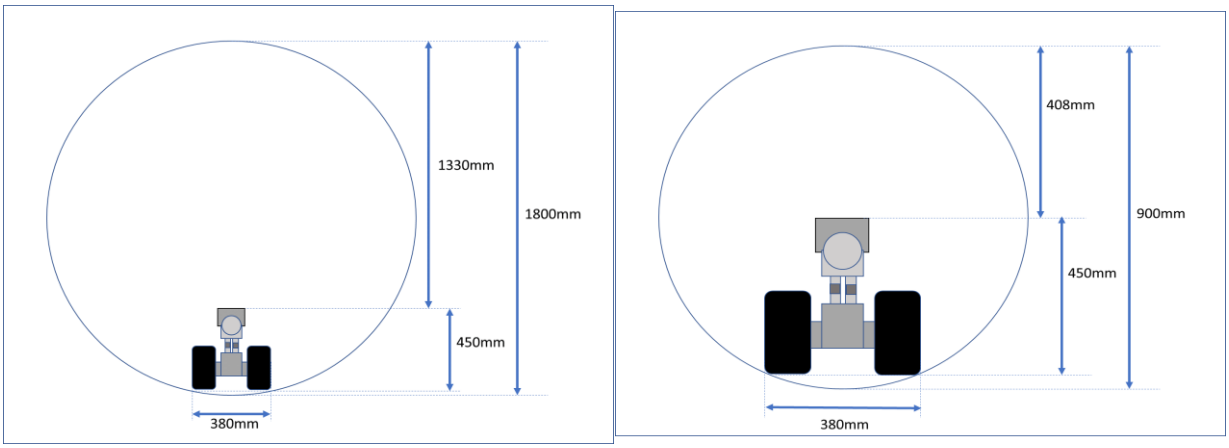

(a) (b)

Figure 3: Schematic diagram of the IPIT tractor inside the two sewer pipe at (a) Jalan Eunos of pipe diameter 1800mm and (b) Tech Park Crescent of pipe diameter 900mm.

There are several criteria used in the design of the on-site setup, and these are discussed below.

(1) Minimum focus distance between the lens and the pipe crown.

The minimum distance between the infrared camera and the crown of the pipe is restricted by the focal length of the camera lens. A 9mm wide angle lens with a minimum focus distance of 32mm

was used, which meant that the minimum distance between the infrared camera and the crown of the pipe should be at least 32mm. As shown in Figure 3, the designed distances between the infrared camera and the crown of the two different sewer pipes are 1330mm and 408mm for the Jalan Eunos and Tech Park Crescent sites respectively, which far exceeds the required 32mm focal length.

(2) Minimum detectable size of defects.

The minimum detectable size of defects depends on the spatial resolution of the infrared camera lens and the distance between the infrared camera and the target area. The minimum detection size of an infrared camera lens is determined by multiplying the instantaneous field of view (IFOV) by the distance in metres from the lens to the pipe crown. According to the specification of the infrared camera FLIR Tau 2 640, the IFOV is 1.889mrad, and therefore the minimum detectable size of defects is 1.889mrad x 1.33m = 2.5mm in the Jalan Eunos pipe and 1.889mrad x 0.408m = 0.77mm in the Tech Park Crescent pipe, which is considered very satisfactory for debond detection.

(3) In-pipe wind speed.

Another factor for consideration is the in-pipe wind speed, which could yield undesirable convection effects. According to the ASTM D-4788 [32], infrared thermography survey should not be carried out in a wind speed higher than 6m/s. Beyond this limit, the wind speed may affect the temperature distribution of defects and intact areas because of convection. In-pipe wind speed was measured on-site with an anemometer and was found to be about 0.5m/s, which is much lower than the 6m/s limit. It therefore follows that the effect of in-pipe wind velocity is negligible in this experiment.

(4) Speed of CCTV tractor

The fourth factor for consideration is the speed of the CCTV tractor carrying the IR camera, since it will affect the quality of thermal images captured by the infrared camera. Unlike normal optical cameras, the data capture frequency of IR camera Tau 2 640 is only 7.5Hz. Therefore, if the tractor moves at higher velocities the thermal images may be blurred. The results of trial test showed that 12m/min was too fast and the captured thermal images were rather blurred. Therefore, the speed was reduced to 6m/min during the whole course of the experiments.

(5) Heat source

In this study, both active and passive thermography were applied in the on-site experiments. As previously mentioned, passive thermography does not require any external heat source during the process of measurement. In contrast, for active thermography, an external heat source is required. In this study, a 15kW heat blower was used to heat up the sewer pipe. The temperature of the heat blower was set to 45^{o}C. The sewer temperature and liner temperature were monitored by a digital thermometer with K-type thermocouple. The heating time and the power of the heat blower are further considerations to be taken into account for debond detection by IRT as they affects the temperature contrast for defect detection. Sufficient temperature contrast is always a critical factor for defect detection by IRT. The schematic diagram of the on-site setup for active thermography is shown in Figure 4. The set-up was the same as active thermography for passive thermography except for the installation of the heat blower.

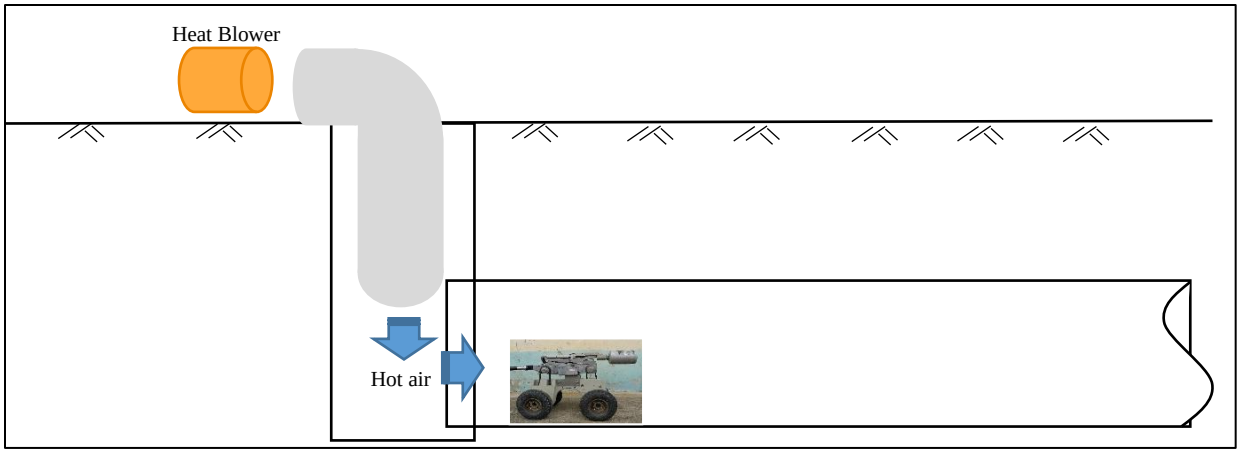

Figure 4: Schematic diagram of on-site setup for active thermography

Figure 5: On-site photos with the setup of heat blower blows hot air of 45ºC into the sewer pipe and the CCTV tractor mounted with IR-camera

As shown in Figure 5, the heat blower was placed next to a manhole. Hot air was blown into the sewer pipe from the surface in order to avoid the potential risks associated with placing a heat source (e.g. light bulb/heater) inside the sewer pipe, while the setup also provides an even heat distribution inside the pipe. The temperatures of the sewer and liner were monitored during the heating up process to avoid any overheat inside the sewer pipe, as well as to ensure that a sufficient temperature difference (i.e. >1ºC) between the sewer and the liner was achieved. The proposed IR camera for the experiment has a temperature resolution of 0.05ºC at room temperature. In this study the test was therefore started when the measured sewer and liner temperatures had risen by

more than 1°C and, in reality, the temperature was actually raised by around 3°C for testing in this case.

5. Development of In-house Infrared- Size Estimation (IR-SE) Program

An in-house program specifically designed for size estimation based on infrared images (IR-SE) was developed by using a virtual programming platform – LabVIEW. It enables estimation of defect size on each captured thermal image. The interface of the IR-SE program is shown in Figure 6. It includes displays of (A) the raw thermal image, (B) processed image and (C) raw thermal image with identified defects. The image processing techniques used in the IR-SE program are discussed in the following section. A debond defect size threshold can be set, such that any defects larger than that size will be highlighted and defined as debonds.

The IR-SE program enables the user to identify the region of interest (ROI) and the size estimation process will only be carried out within the ROI. This can significantly reduce the processing time. The program is compatible with both comma separated value (CSV) and 8bit image data formats.

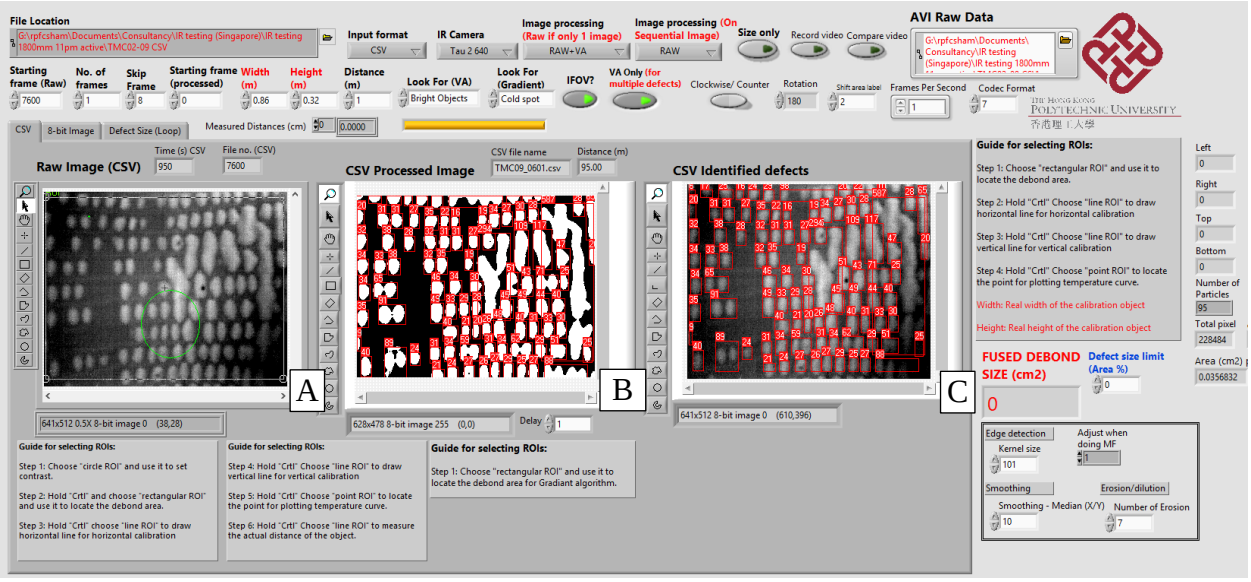

Figure 6: Interface of IR-SE program build up by LabVIEW Instrument.

5.1. Image Processing

In the IR-SE program, several image analysis techniques have been applied for debond detection. The major image processing steps applied involved the following techniques: (1) edge detection, (2) smoothing and (3) the removal of small-scale noise using an erosion and dilution function. Edge detection was applied when a thermal image was imported to the program. A raw thermal image (Figure 7 (a)) processed by the above image processing steps is presented in Figure 7.

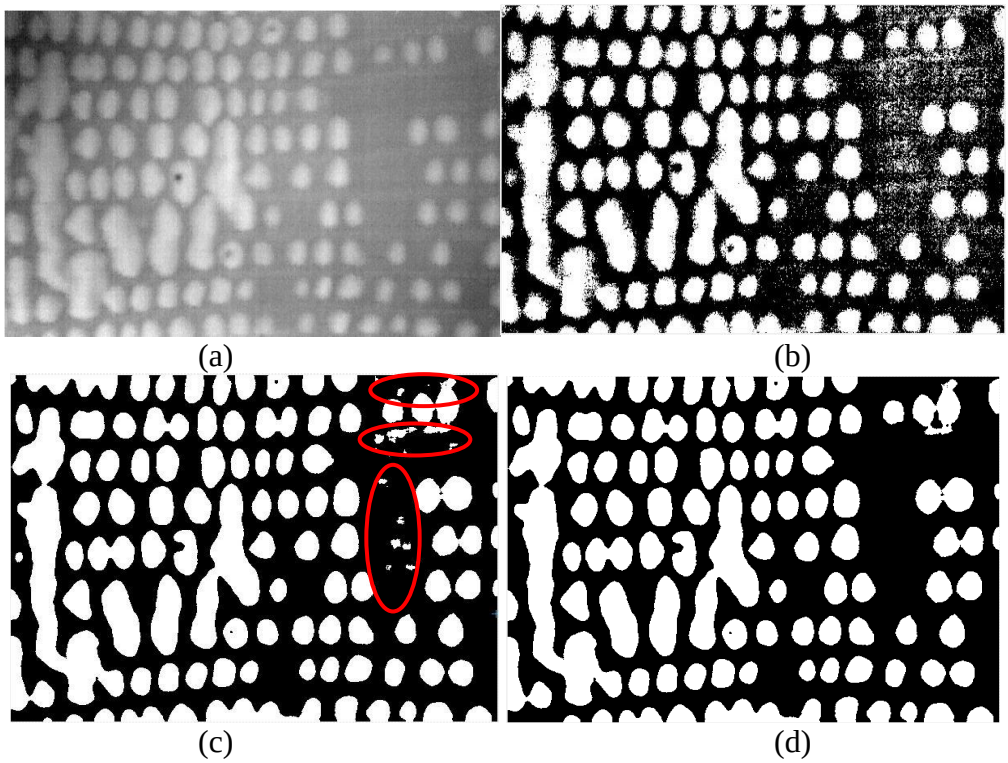

Figure 7: (a) Raw image; (b) Edge detection - Laplacian; (c) Smoothing – Median Filtering (d) Lowpass filter.

Edge detection

There are several common image processing methods for edge detection, such as Laplacian filtering, differentiation filtering, Prewitt filtering, Sobel filter, Roberts filter and Canny filter [33]. Laplacian filtering was used in this program for edge detection. In contrast to other filters such as Prewitt, Sobel and Roberts, it is a second order derivative mask that outlines more details of the thermal images that are then used to identify defects analogous to the gradient computational

algorithm in Lai's study [34]. The latter was shown to have an accuracy of about 70-85% with respect to the size estimation of debonds in external wall tile/render, which is a composite system similar to the liner composite tested in this study. Laplacian filtering can be divided into two types: positive and negative [35]. In this study, the negative and diagonal operators were used and an example of a 3x3 kernel model is shown below:

a	d	c
b	***x***	b
c	d	a

(a)

-1	-1	-1
-1	8	-1
-1	-1	-1

(b)

Figure 8: (a) Laplacian 3x3 kernel and (b) negative and diagonal 3x3 kernel operator.

The thickness of detected edges increased when the size of the kernel increased [36]. Therefore, a clearer image of the outlined defects' shapes will be formed when a larger kernel size number is used (i.e. 9x9 to 101x101), as shown in Figure 9:

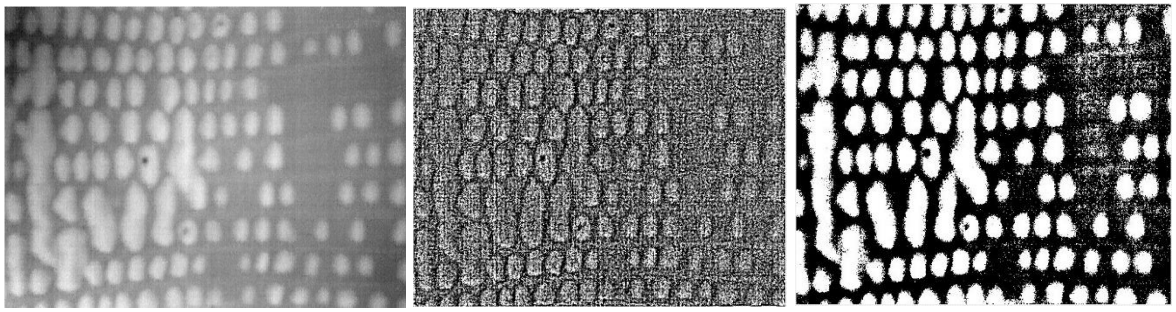

(a) (b) (c)

Figure 9: (a) Raw thermal image; (b) Laplacian kernel of 9x9; (c) Laplacian kernel of 101x101.

To move beyond simply identifying the outline of debonds, a large Laplacian kernel is proposed in order to form a solid shape as shown in Figure 7 (c).

Smoothing

After edge detection, smoothing is recommended for eliminating noise in thermal images. As mentioned by Mlsna, 2009 [35], the drawback of using a Laplacian filter is that it is extremely sensitive to noise because it works with a second order derivative. Therefore, it is necessary to eliminate noise after Laplacian filtering. As suggested by Ibarra-Castanedo's team [33], median filtering is well-suited to the smoothing of noise particular to thermal images because it is good for removing spiky noise. It is a low-pass filter that assigns each pixel with the median value of its neighbours [36], and hence can remove isolated pixels and thereby effectively reduce detail.

Morphology – erosion and dilution

Basically, after smoothing, any debonds present are imaged with more rounded oval shapes without spiky noise as shown in Figure 7 (c). However, after smoothing we can still see some small-scale noise in the processed image (marked with red circle in Figure 7 (c)). In order to remove this residual noise, an optional morphology technique, combining erosion and dilation functions, was therefore applied[37]. For erosion, the contour, i.e. the size of the objects, will be reduced as the number of erosion function iterations is increased. Small objects can therefore easily be removed by increasing the number of iterations of the erosion function. However, the disadvantage is that it may also reduce the sizes of other objects that do not need to be eliminated. The dilution function can increase the contour of objects with higher intensities by increasing the number of iterations. Therefore, a dilution function was applied after the erosion function in order to restore the size of objects that needed to be retained. By this combined method, the small objects, which are removed by the erosion function, will not appear again, whereas the targeted objects (i.e. defects) will be returned to their normal size by the dilution function [37]. The result is shown in Figure 7 (d).

The detailed settings of different image processing procedures used for detecting debonds and water seepages in this study are listed in Table 3:

Table 3: Settings of image processing procedures

	Edge Detection – Laplacian filtering		**Smoothing - Median filtering**		**Advanced Morphology – Remove small objects**	
	Debond	Water seepage	Debond	Water seepage	Debond	Water seepage
Kernel	101 x 101	59 x 59	-	-	-	-
Filter size	-	-	10 x 10	2 x 2	-	-
Iteration	-	-	-	-	5	7

The shape of the debonds can clearly been seen after the above image processing steps. Following image processing, size estimation can then be carried out because the grayscale thermal image has been changed to a binary image in which only values of 0 or 1 are presented. The debonds' sizes can thus be calculated by counting the numbers of pixels with values of 0 (hot spot) or 1 (cold spot).

5.2. Image Analysis - Size estimation

As mentioned before, the grayscale images were converted to binary images in which debond areas were assigned a 0 value. Particle analysis can hence be applied to calculate the numbers of 0 value pixels and estimate the debond size. Before calculating the size, the pixel scale to real object size was appropriately set. There are two methods available in the IR-SE program: (1) by length calibration or (2) by calculating IFOV. For the length calibration method, width and height was measured and then fitted into the thermal image (raw image) in the program. The program will calculate the estimated size by referring to the referenced width and height. For the IFOV method, the actual pixel size was calculated by multiplying the IFOV of the lens by the distance from the lens to the pipe crown. The program can calculate the counted number of pixels of the targeted

debond area. In this study, the surface offered no measurable reference width or height (i.e. length calibration method), and the IFOV method was therefore used to determine the size of debonds.

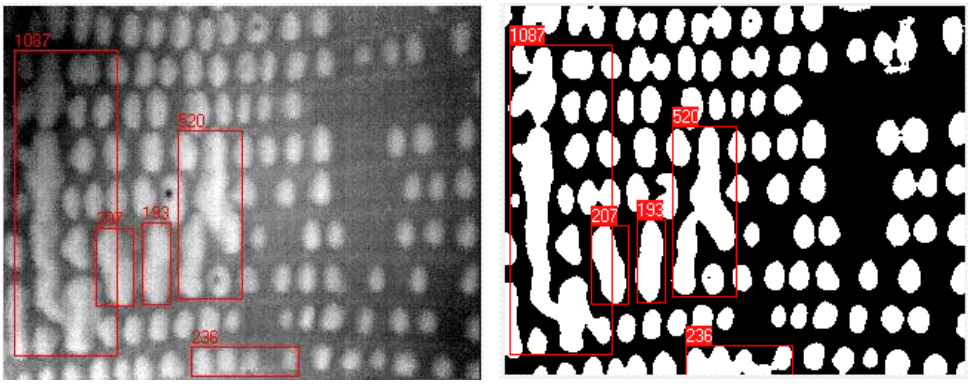

(a) (b)

Figure 10: Identification of targeted debond area by IR-SE program (a) raw thermal image and (b) binary image of the corresponding thermal image (a).

The IR-SE program enables automatic detection of targeted debond areas to support maintenance decision-making. Unlike CCTV survey, which is highly subjective based upon individual interpretation, the IR-SE program automatically identifies any debond areas that exceed the thresholds set for the detection criteria. A targeted percentage area of debond relative to the overall image area (i.e. the maximum debond size that may require further attention in future maintenance works) can be set in the program. In the example shown in Figure 10, the debond size threshold was set to an area larger than 1.1% of the entire thermal image. Five debonds were highlighted automatically by the program and are identified on both the raw thermal image and binary image, while other objects (bubble shapes) were considered to be construction details of the AKS HDPE liner as shown in Figure 2. This threshold and its absolute value can be adjusted by the user, thereby giving a clear watershed of judgement (i.e. debond/no debond). The estimated sizes are also shown next to each red rectangle in cm^2 in the binary image (Figure 10) (i.e. sizes of defects from left to right as follows: 1087cm^2, 207cm^2, 193cm^2, 520cm^2, 236cm^2). Since the curvature of the pipeline

353 is neglected in this study, these sizes are estimated and accurate debond size calculation if proposed
354 for later study.

355 6. Results and Discussion

356 The results of the application of passive and active infrared thermography for condition assessment
357 in both 900mm and 1800mm sewer pipes are presented below. According to the results, only the
358 first 10m near the hot air inlet produced clearer observations of lining defects. This may due to the
359 use of an underpowered heat blower or a period of preheating that was insufficient to heat up the
360 whole length of pipe. Therefore, further studies on the preheating process are recommended. Some
361 representative thermal images from the tests are presented with their corresponding visual images
362 captured by the CCTV survey for comparison.

363 *6.1. IR results on 900mm and 1800mm diameter sewage pipe*

364 Several lining defects were observed during the thermography survey. Theoretically-speaking,
365 active thermography is better-suited to the detection of debonds, while passive thermography is
366 usually used for detecting water seepage. Therefore, the results of both water seepage and lining
367 debond detections will be presented for 900mm and 1800mm diameter sewage pipes, with a
368 particular focus on those defects that could not be observed in visual images but can be seen on
369 thermal images.

370 *Debond detection by active thermography:*

900mm sewer pipe

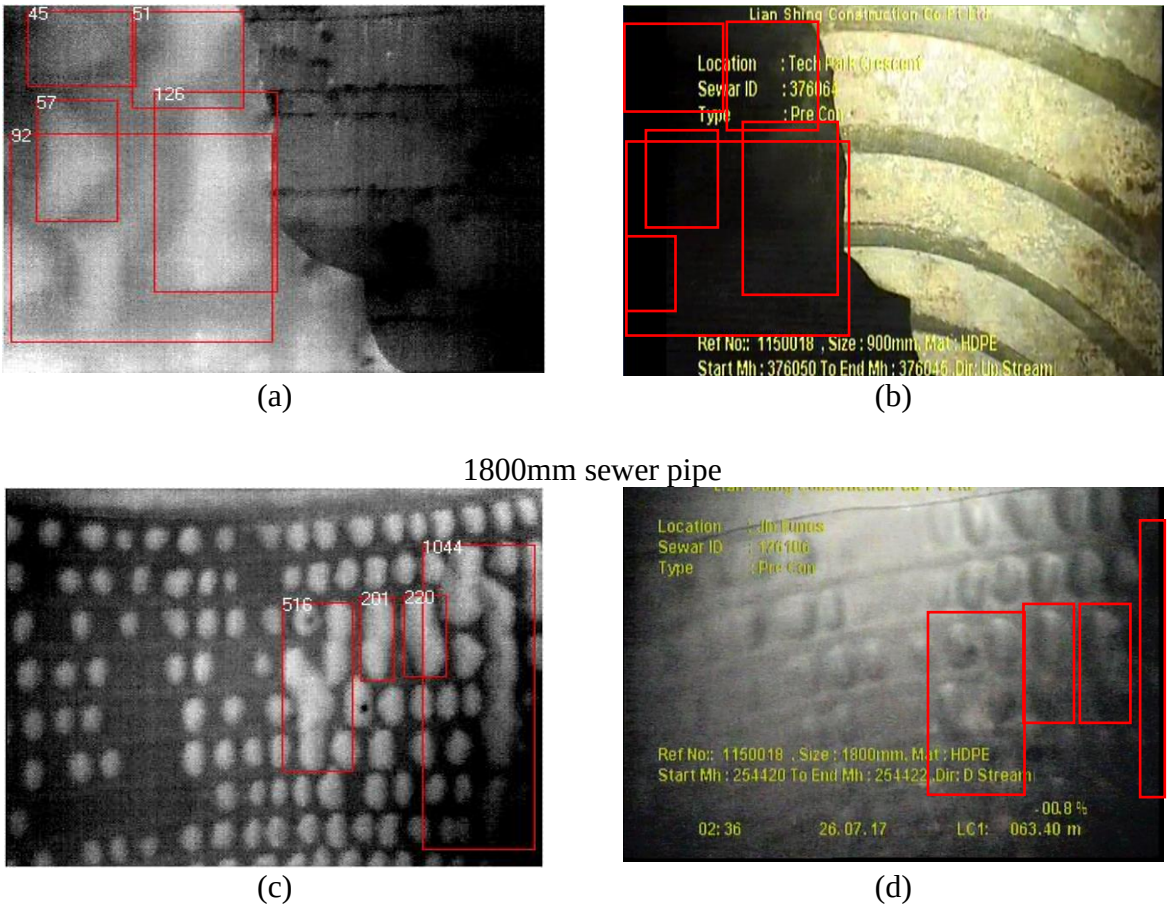

Figure 11: Identification of debond area by IR-SE program (a) raw thermal image and (b) the corresponding CCTV visual image in 900mm sewer pipe; (c) raw thermal image and (d) the corresponding CCTV visual image in 1800mm sewer pipe.

As shown in Figure 11, the debond areas in the 900mm and 1800mm sewer pipes were detected as hot spots (white areas) in the grayscale thermal image. In the 900mm sewer pipe, suspected debond areas are bounded by red rectangles in Figure 11 (a) and (b). These areas can be observed in the thermal image but could not be detected in the CCTV visual image. In the 1800mm sewer pipe, many small white bubbles are observed in Figure 13 (c) and (d). As mentioned before, unlike the 900mm sewer pipe, the 1800mm sewer pipe is a built-in (anchor knob sheet) AKS HDPE sewer pipe. The white bubbles observed in the thermal images are similar to the anchor knob pattern of the AKS HDPE liner in Figure 2. Some of those bubbles are joined together to form bigger debonds, which are bounded by red rectangles in Figure 13 (c) and (d).

Water seepage detection by passive thermography:

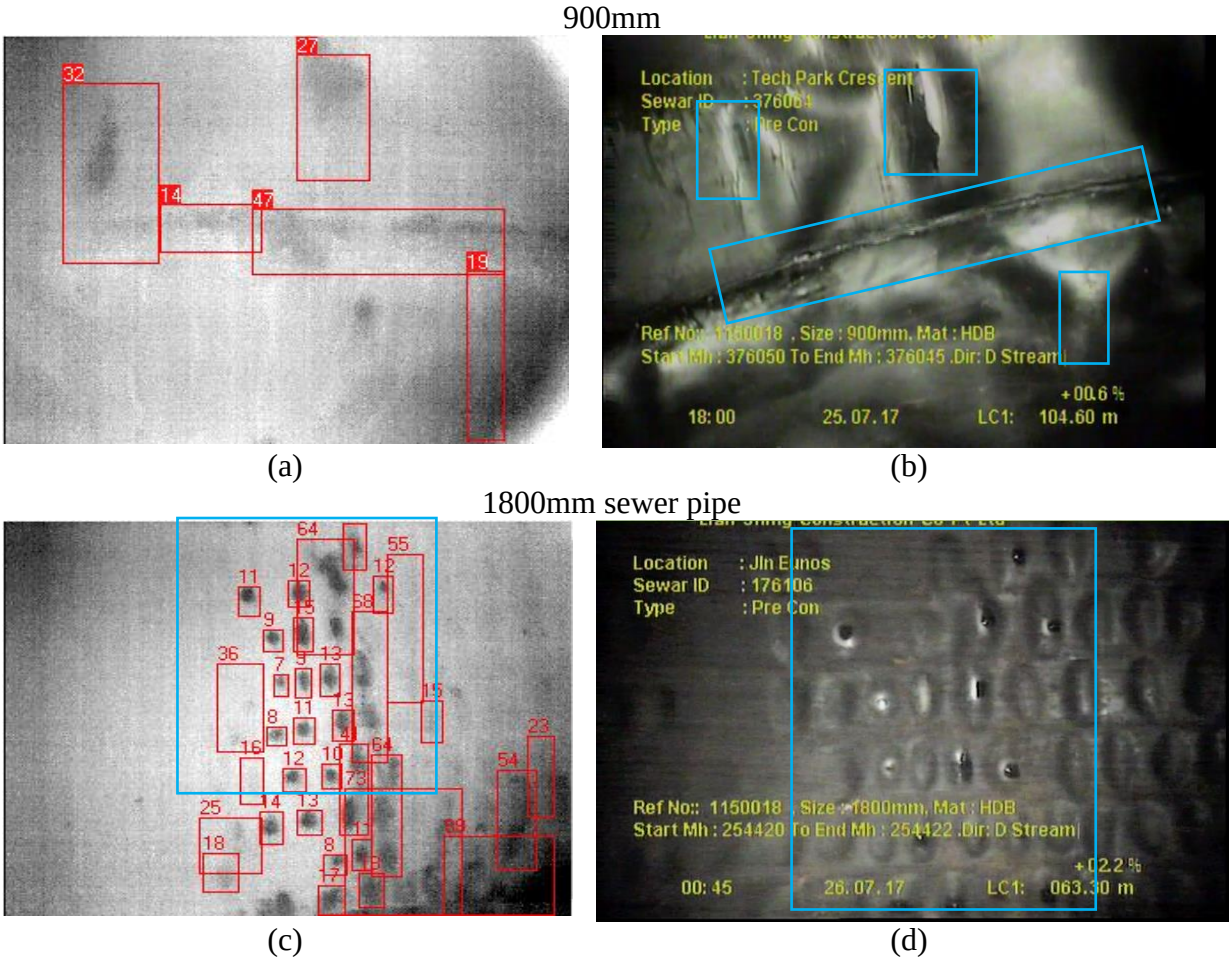

Figure 12: Identification of suspected water seepage area by IR-SE program (a) raw thermal image and the corresponding CCTV visual image (b) in 900mm sewer pipe; (c) raw thermal image and the corresponding CCTV visual image (d) in 1800mm sewer pipe.

As shown in Figure 12, suspected water seepage areas (bounded by a blue rectangle) are picked up in thermal images but it can hardly be identified in the visual image. In the 900mm sewer pipe, suspected water seepage areas are identified at the joints of the sewer pipe in the thermal image in Figure 12 (a), but cannot easily be identified in the visual image in Figure 12 (b). In the 1800mm sewer pipe, signs of water seepage can be observed in both thermal and visual images (Figure 12 (c) and (d)). However, more clear dots indicating water seepage can be observed in the thermal

image (Figure 12 (c)) because our view was not distracted by the liner bubbles and uneven lighting observed in the visual image shown in Figure 12 (d).

6.2. Comparison of results between Active Thermography, Passive Thermography and CCTV Survey

In this section, only the results of passive and active thermography in the 1800mm pipe are presented (Figure 13). This is because the pattern of lining debonds in the 1800mm pipe are more regular and can therefore be more easily compared. Also, thermal images captured in the 1800mm pipe have a better field of view because the distance between the infrared camera and the crown of the sewer pipe is greater than that in the 900mm sewer pipe. As a result of the infrared camera's 7.5Hz frequency, thousands of thermal images were captured during the test, and therefore only a selection of the more remarkable thermal images were selected for comparison. .

1800mm sewer pipe

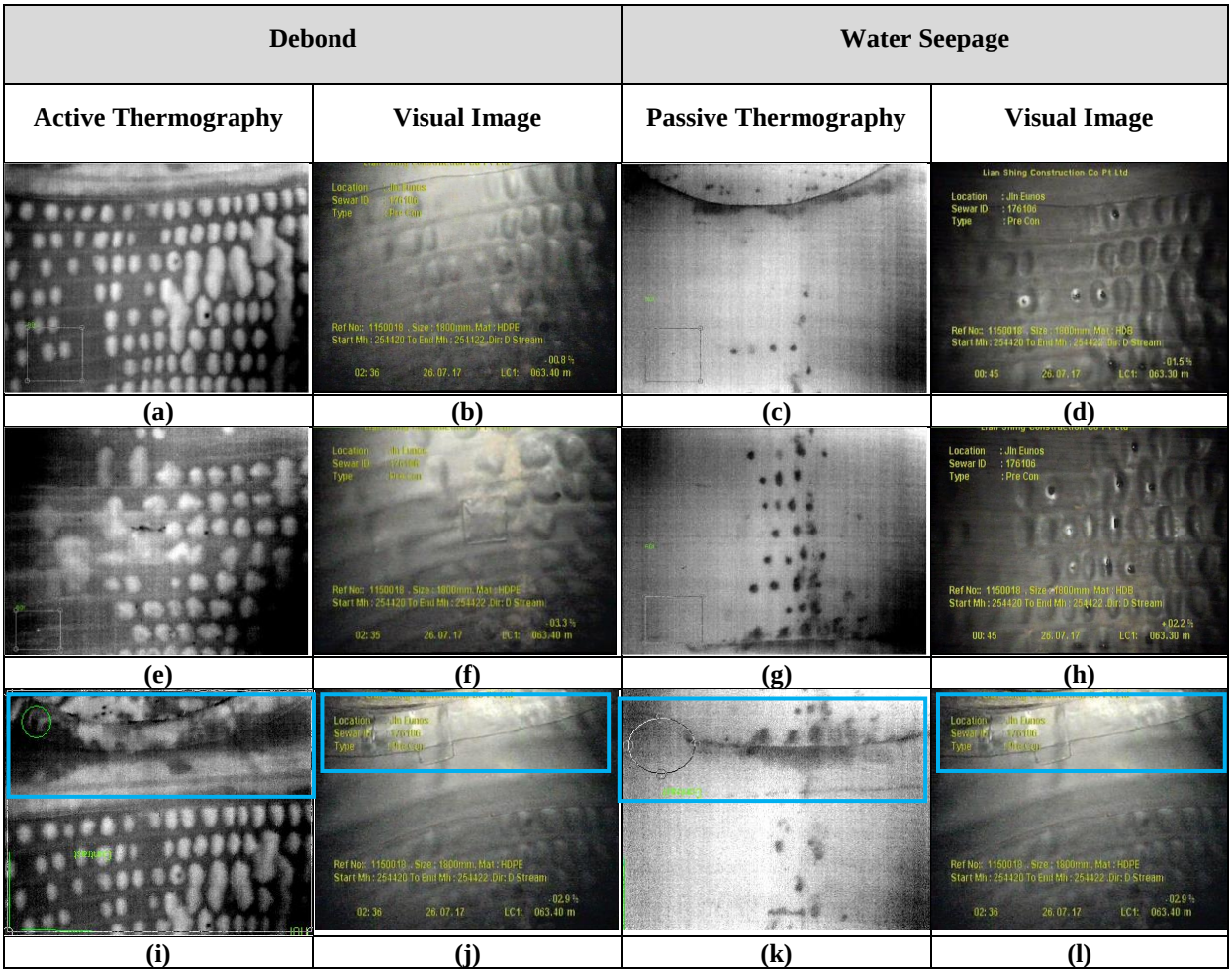

Figure 13: Selected thermal images and their corresponding visual image captured by CCTV in 1800mm diameter sewer pipe for comparison of active and passive thermography.

From the above results, it shows that liner debonds (white areas) can easily be observed in thermal images produced by active thermography (Figure 13 (a-b), (e-f), (i-j)), while the debonds cannot be seen in thermal images yielded by passive thermography (Figure 13 (c-d), (g-h), (k-l)). On the other hand, water seepage areas (black dots) were observed by passive thermography, as shown in (Figure 13 (c-d), (g-h) and (k-l)). In general, water seepage areas could be more clearly observed in passive thermography since there are fewer distracting debonds (white areas) than are detected by active thermography. However, in some cases the water seepage areas are sharper in thermal images captured by active rather than passive thermography as is shown in Figure 13 (i-l) bounded

by a blue rectangle. The infrared camera's focus is improved by increasing the temperature difference produced by a heat source. Moreover, sharper thermal images are captured by active thermography while thermal images from passive thermography are relatively blurred.

7. Limitation of IPITS

The limitation of IPITS is that images of the interior wall can only be obtained above the water surface in the case of sewer and water pipes. Besides, in common with CCTV, the movement of the tractor when travelling along the pipeline causes unsteady camera movement. That instability affects the quality of captured thermal images. Lastly, another limitation of the technique is the lack of geometric references inside the pipe.

8. Conclusion and Recommendation

In conclusion, this paper presents a case study using Infrared Thermography for In-pipe lining debond detection, where both active and passive thermography were applied for imaging and diagnosis. The paper presentedthe entire process of system design and program development and discussed the on-site testing results . We are delighted to have achieved remarkable results in terms of debond and water seepage detection in sewer pipes using both passive and active thermography. Several highlights are listed as below:

- Preliminary on-site setup with both passive and active thermography were designed;
- An IR-SE program for estimating defect size was developed. The program allows automatic defect identification of targeted debond size;
- An algorithm for automatic defect detection and size estimation was developed by implementing different combinations of image processing techniques;

- Suitable speeds of CCTV tractor were tested, and 6m/min is recommended for infrared thermography survey in sewer pipes;
- The results of infrared thermography for detecting liner debonds and water seepage areas by both active and passive themrography were presented and compared. Active thermography gives clearer thermal images because of higher elevated temperature differences. It also allows more effective inspection of liner debonds. On the other hand, water seepage areas can be identified by passive thermography.

Based upon the findings of this study, several recommendations concerning instrumentation and testing procedures for further implementation of infrared thermography survey for condition diagnosis of underground sewer liners are offered.

On instrumentation:

- Install two IR cameras – set up for 10-12 o'clock and 12-2 o'clock viewing positions;
- Using 2 cameras helps maximize the angle of field of view;
- Mount IR cameras in sealed, waterproof housings;
- Use an additional (CCTV) camera together with the IR cameras for better synchronization between the IR and visual images;
- Increase IR frame rate to allow faster tractor traverse speed while maintaining image quality, especially in sewer tunnel with higher flow velocity (typical of tunnel sewers vs. minor/trunk sewers);
- Trials of mounting different heat sources on the CCTV tractor along with the IR camera are recommended in order to heat up the inner pipe more evenly throughout the whole length of pipe.

On testing procedures:

- Heating method during active IR can be improved, for example for ordinary city sewer, upstream/downstream connections could be plugged to trap air flow, thereby making it easier to achieve required temperature up to 45 deg C;
- For deep sewer tunnels, other heating means such as impulse heating methods or prolonged heating shall be considered;
- Specifications for infrared thermography survey in sewer pipes, such as maximum allowable pixel resolution in the images as a function of distance between the liner and the IR camera, are to be studied.

This case study serves as a pilot test for future extensive and regular application of infrared thermography for condition diagnosis of underground sewer liners. The detection of debond size and identification of locations with water seepage serve as a reference for engineers to plan for future maintenance schedules. Infrared thermography survey results provide clear pictures of debond size and also early warning of the formation of hidden defects without visible surface scars. Further studies aimed at investigating optimum heating periods, defect characterisation of lining defects and different imaging processing techniques are recommended. It is also recommended that IRT surveys are carried out with other non-destructive condition diagnosis techniques for cross-referencing purposes.

Acknowledgement

The authors gratefully acknowledge Singapore's Public Utility Board (PUB) for providing testing sites and Singapore's Pipeline Inspection and Services Company for their on-site coordination and experimental support.

References

[1] Hadj-Meliani ME, A.; Sadou, M.; Bouledroua, O.; Azari, Z.; Pluvinage, G. Degradation of sewage pipe caused sinkhole: a real case study in a main road. 22nd French Conference of Mechanics. Lyon2015.

[2] McKirdy EE, S. L. Dozens dead as Taiwan gas explosions tear up streets. U. S. A.: CNN; 2014.

[3] Hao T, Rogers CDF, Metje N, Chapman DN, Muggleton JM, Foo KY, et al. Condition assessment of the buried utility service infrastructure. Tunnelling and Underground Space Technology. 2012;28:331-44.

[4] Kirkham R, Kearney PD, Rogers KJ, Mashford J. PIRAT—A System for Quantitative Sewer Pipe Assessment. 2000. p. 1033-53.

[5] OFWAT. Out of Sight - Not Out of Mind: OFWAT. 13th Report of Session2004.

[6] American Society of Civil E, Existing Sewer E, Rehabilitation Task F, Environmental, Water Resources I. Existing sewer evaluation and rehabilitation. 3rd ed.. ed. Alexandria, Va. : Reston, Va. : New York: Alexandria, Va. : WEF Press : Water Environment Federation ; Reston, Va. : American Society of Civil Engineers/Environmental and Water Resources Institute ; New York : McGraw Hill; 2009.

[7] Eiswirth MH, C.; Hotzl, H.; Schneider, T.; Burn, L. S.; . Pipe Defect Characterisation by Multi-Sensor Systems. 18th International Conference No-Dig 2000. Perth, Western Australia2000.

[8] Chae MJA, D. M. Neuro-fuzzy approaches for sanitary sewer pipeline condition assessment. Journal of Computing in Civil Engineering. 2001;15:4-14.

[9] Koo D-H, Ariaratnam ST. Innovative method for assessment of underground sewer pipe condition. Automat Constr. 2006;15:479-88.

[10] Read GF, Vickridge I. Sewers : rehabilitation and new construction. Repair and renovation. London : Arnold ; New York. N.Y.: London : Arnold ; New York. N.Y. : copublished in North, Central and South America by John Wiley & Sons; 1997.

[11] Hodgkinson A. Low cost solutions for managing large diameter pipelines - high-tech systems for assessment, maintenance and refurbishment. 18th International Conference No-Dig 2000. Perth, Western Australia2000.

[12] Garvey M. 3D Laser Scanning Technology Benefits Pipeline Design The World Isn't Flat. Pipeline & Gas Journal. 2012;239:32-6,8.

[13] Huang M-H, Zang S-S, Ge B, Weng S-L. Method of infrared thermography measurement for temperature field of turbine vane in hot wind tunnel. Hangkong Dongli Xuebao/Journal of Aerospace Power. 2014;29:2679-83.

[14] Bagavathiappan S, Lahiri BB, Saravanan T, Philip J, Jayakumar T. Infrared thermography for condition monitoring – A review. Infrared Physics & Technology. 2013;60:35-55.

519 [15] Bianchi F, Pisello AL, Baldinelli G, Asdrubali F. Infrared Thermography Assessment of
520 Thermal Bridges in Building Envelope: Experimental Validation in a Test Room Setup.
521 Sustainability-Basel. 2014;6:7107-20.

522 [16] Lahiri BB, Bagavathiappan S, Jayakumar T, Philip J. Medical applications of infrared
523 thermography: A review. Infrared Physics and Technology. 2012.

524 [17] Alexis C, Franck B, Didier D, Emmanuel A, Hangseok C. Evaluation of gluing of CFRP
525 onto concrete structures by infrared thermography coupled with thermal impedance. Compos
526 Part B-Eng. 2015;69:350-8.

527 [18] Balaras CA, Argiriou AA. Infrared thermography for building diagnostics. Energy and
528 Buildings. 2002;34:171-83.

529 [19] Bisegna F, Ambrosini D, Paoletti D, Sfarra S, Gugliermetti F. A qualitative method for
530 combining thermal imprints to emerging weak points of ancient wall structures by passive
531 infrared thermography - A case study. Journal of Cultural Heritage. 2014;15:199-202.

532 [20] de Freitas SS, de Freitas VP, Barreira E. Detection of façade plaster detachments using
533 infrared thermography – A nondestructive technique. Construction and Building Materials.
534 2014;70:80-7.

535 [21] Lai WL, Kou SC, Poon CS, Tsang WF, Lai CC. Characterization of the deterioration of
536 externally bonded CFRP-concrete composites using quantitative infrared thermography. Cement
537 and Concrete Composites. 2010;32:740-6.

538 [22] Lai W.L PCS. Durability and debond evaluation of high-rise concrete buildings using
539 infrared thermography. First International Conference on Performance-based and Life-cycle
540 Structural Engineering2012.

541 [23] Lai WL, Lee KK, Kou SC, Poon CS, Tsang WF. A study of full-field debond behaviour and
542 durability of CFRP-concrete composite beams by pulsed infrared thermography (IRT). NDT & E
543 International. 2012;52:112-21.

544 [24] Maierhofer C, Brink A, Rollig M, Wiggenhauser H. Transient thermography for structural
545 investigation of concrete and composites in the near surface region. Infrared Physics &
546 Technology. 2002;43:271-8.

547 [25] Maierhofer C, Brink A, Röllig M, Wiggenhauser H. Detection of shallow voids in concrete
548 structures with impulse thermography and radar. NDT & E International. 2003;36:257-63.

549 [26] Maldague X, Moore PO, American Society for Nondestructive T. Infrared and thermal
550 testing. 3rd ed. Columbus, OH: Columbus, OH : American Society for Nondestructive Testing;
551 2001.

552 [27] Kylili A, Fokaides PA, Christou P, Kalogirou SA. Infrared thermography (IRT) applications
553 for building diagnostics: A review. Applied Energy. 2014;134:531-49.

554 [28] Brown JR, Hamilton HR. Heating methods and detection limits for infrared thermography
555 inspection of fiber-reinforced polymer composites. Aci Mater J. 2007;104:481-90.

556 [29] Maierhofer C, Brink A, Rollig M, Wiggenhauser H. Quantitative impulse-thermography as
557 non-destructive testing method in civil engineering - Experimental results and numerical
558 simulations. Construction and Building Materials. 2005;19:731-7.

559 [30] Ibarra-Castanedo C, Maldague X. Pulsed phase thermography reviewed. Quantitative
560 InfraRed Thermography Journal. 2004;1:47-70.

561 [31] Maldague X. Theory and practice of infrared technology for nondestructive testing. New
562 York: Wiley; 2001.

563 [32] ASTM4788. Standard Test Method for Detecting Delaminations in Bridge Decks Using
564 Infrared Thermography. 2013.

565 [33] Ibarra-Castanedo C, González D, Klein M, Pilla M, Vallerand S, Maldague X. Infrared
566 image processing and data analysis. Infrared Physics and Technology. 2004;46:75-83.

567 [34] Lai WW-L, Lee K-K, Poon C-S. Validation of size estimation of debonds in external wall's
568 composite finishes via passive Infrared thermography and a gradient algorithm. Construction and
569 Building Materials. 2015.

570 [35] Mlsna PA, Rodríguez JJ. Chapter 19 - Gradient and Laplacian Edge Detection A2 - Bovik,
571 Al. The Essential Guide to Image Processing (Second Edition). Boston: Academic Press; 2009.
572 p. 495-524.

573 [36] Instrument N. IMAQ Vision Concpets Manual. Texas: National Instruments Corporation;
574 2003.

575 [37] Kwon KSR, S. Practical Guide to Machine Vision Software: An Introduction with
576 LabVIEW: John Wiley and Sons; 2014.

577